J. Korean Inst. Electr. Electron. Mater. Eng.
Vol. 38, No. 4, pp. 376-382 July 2025
doi: https://doi.org/10.4313/JKEM.2025.38.4.4
ISSN 1226-7945(Print), 2288-3258(Online)

Regular Paper

Dielectric Characteristics of $(BaCaSr)(Ti_xZr_{1-x})O_3$ Dielectric Ceramic with Temperature Compensation Capacitor Characteristics

Yoo Jung Choi, Hong Sun Lee, and Jung Rag Yoon

R&D Center, Samwha Capacitor, Yongin 17118, Korea

(Received January 16, 2025; Revised February 4, 2025; Accepted February 6, 2025)

Abstract: This study developed a dielectric composition for high-capacitance MLCCs with C0G and U2J temperature compensation characteristics (Class I) under reducing conditions. The potential application of this composition in high-permittivity class I MLCCs was examined. Using $(Ba_{0.24}Ca_{0.16}Sr_{0.6})(Ti_xZr_{1-x})O_3$. XRD analysis showed that secondary phases like Sr_2TiO_4 and TiO_2 formed at higher Ti content, affecting the stoichiometric balance. Adjusting the Ti/Zr molar ratio resulted in a dielectric constant of 41.2 ~ 105, a dielectric loss of 0.082 ~ 0.174%, and insulation resistance above 1.6×10^{13} ohms at 25°C. The TCC shifted from C0G to U2J as the Ti/Zr ratio increased, but the composition enabled the design of high-capacitance and high-voltage MLCCs with favorable dielectric and electrical properties.

Keywords: Dielectric properties, Multi-layer ceramic capacitor, Insulation resistance, C0G and U2J temperature compensation characteristics

1. INTRODUCTION

With the rapid development of the electronics industry and the expansion of IoT, cloud computing, artificial intelligence (AI), and eco-friendly automobile markets, the demand for improved performance and reliability of electronic components has significantly increased [1-3]. Particularly, in power conversion circuits and high-frequency applications, multilayer ceramic capacitors (MLCCs) have become essential components due to their ability to support high capacitance and high voltage while maintaining stable electrical properties and low dielectric losses under varying temperature conditions. Temperature-compensating MLCCs, categorized as C0G and U2J grades, provide excellent performance across a wide temperature range (-55°C to 125°C) by exhibiting linear responses to temperature and voltage changes. C0G dielectrics, in particular, are widely used in high-reliability applications such as aerospace, medical devices, and high-frequency circuit impedance matching due to their low dielectric losses and outstanding durability. C0G MLCCs are essential in high-voltage power conversion circuits like switching power supplies, DC-DC converters, and inverters due to their low voltage dependence, excellent high-frequency characteristics, and low loss, maximizing power efficiency. The rise of SiC and GaN power semiconductors has increased the demand for MLCCs in high-frequency, high-voltage applications. Technological advancements have enabled high-capacitance, high-voltage C0G MLCCs to replace traditional film capacitors, offering superior stability, reliability, and compactness. Their ability to maintain stable performance under extreme conditions makes them ideal for electric vehicles, industrial power supplies, and

✉ **Jung Rag Yoon; yoonjungrag@samwha.com**

RF applications, driving their widespread adoption. Traditionally, C0G-based MLCCs employed precious-metal electrodes (PMEs) such as those in Ba-Nd-Ti systems, which exhibit high dielectric constants (ε_r = 60 ~ 100) [4]. However, to reduce manufacturing costs, the use of base-metal electrodes (BMEs) such as nickel (Ni) and copper (Cu) has increased. These electrodes require sintering processes in a reducing atmosphere, which often introduces oxygen vacancies, leading to increased electrical conductivity in the dielectric materials. Therefore, the development of reduction-resistant dielectric materials capable of maintaining stable properties under reducing conditions is crucial. Among reduction-resistant dielectric materials, $CaZrO_3$ ceramics, which possess a perovskite structure, stand out with a dielectric constant (ε_r) of ~27, a high-quality factor (Q·f) of 16,543 GHz, an insulating resistivity (ρ) of 10^{12} Ω·cm, and a resonant frequency temperature coefficient (TCf) of ~19.98 ppm/°C. These properties make $CaZrO_3$ a promising material for high-performance applications. Additionally, $SrZrO_3$ exhibits a slightly higher dielectric constant of ~30, a Q·f of 13,600 GHz, and a TCf of ~60 ppm/°C. Adjusting the Ca/Sr ratio in $(Ca_xSr_{1-x})ZrO_3$ ceramics influences the crystalline structure and dielectric properties [5-7]. An increased Ca content reduces the sintering temperature and increases grain size; however, excessive Ca can lead to impurity phases such as ZrO_2 or $CaZr_4O_9$, which degrade dielectric properties. To address this issue, studies have focused on tuning non-stoichiometric compositions to minimize impurities and optimize dielectric properties. To achieve high-capacitance MLCCs with temperature-compensating properties, perovskite ceramics such as $CaZrO_3$, $(CaSr)ZrO_3$, and $(CaSr)(ZrTi)O_3$ have garnered attention [8-10]. Based on reference [11-13], a $(BaCaSr)(ZrTi)O_3$ composition with a high dielectric constant was designed to develop a temperature-stable dielectric material with enhanced permittivity. $BaZrO_3$, exhibiting a relatively higher dielectric constant (~36) compared to $CaZrO_3$ and $SrZrO_3$, has been identified as a key component for optimizing both dielectric performance and thermal stability in $(BaCaSr)(ZrTi)O_3$ systems. In this study, we investigated the electrical properties and microstructure of the $(Ba_{0.24}Ca_{0.16}Sr_{0.6})(Ti_xZr_{1-x})O_3$ composition by adjusting the Ti/Zr molar ratio. The goal was to optimize dielectric and temperature properties under reducing sintering conditions and evaluate the potential applicability of the material for high-capacitance, high-voltage, high-performance MLCCs.

2. EXPERIMENTAL

The $(Ba_{0.24}Ca_{0.16}Sr_{0.6})(Ti_xZr_{1-x})O_3$ ceramics were synthesized using conventional solid-state ceramic processing techniques. The starting materials, $BaCO_3$ (99.9%, Sakai Chemical Co.), $SrCO_3$ (99%, 9.9%, Kojundo Chemical Laboratory Co.), $CaCO_3$ (99%, Kojundo Chemical Laboratory Co.), ZrO_2 (99.9%, Kojundo Chemical Laboratory Co.) and TiO_2 (99%, ishihara chemical Co.), were weighed in stoichiometric ratios and mixed thoroughly for 24 hours using distilled water and zirconia media in plastic containers. The mixed powders were calcined at 1,150°C for 2 hour to ensure complete reaction. As additives, Mn_3O_4, Al_2O_3, and MoO_3 were incorporated to suppress insulation resistance degradation and enhance dielectric properties during sintering in a reducing atmosphere, while $(Ba_{0.4}Ca_{0.6})SiO_3$ glass powder was added to lower the sintering temperature and improve insulation resistance characteristics. The prepared calcined powder, along with additives, zirconia balls, and deionized water, was mixed and milled using a bead mill to ensure uniform particle size and dispersion. The milled powder was subsequently dried and further dispersed using a basket mill with polyvinyl butyral (PVB) as a binder, a dispersant, and a toluene/ethanol solvent mixture to produce a homogeneous slurry. This slurry was cast into green sheets with a thickness of 30 μm using the doctor blade method on a PET film substrate. Twenty-five layers of the green sheets were stacked and compressed using an isostatic press to form compacted bars. The compacted bars were then cut into cylindrical samples with a diameter of Φ 15 mm. These samples underwent a binder burnout (BBO) process to remove organic components, followed by sintering at 1,320°C for 2 hours in a reducing atmosphere with an oxygen partial pressure of 10^{-12} ~ 10^{-13} atm. After sintering, the samples were reoxidized at 950°C for 1 hour to enhance properties. Ag electrodes were printed onto the sintered samples and subjected to a thermal treatment before performing dielectric and electrical property measurements. The dielectric properties, including dielectric constant (ε_r) and dielectric loss (tan δ), were measured using an LCR meter (HP 4284A) in the frequency range of 100 Hz

to 2.0 MHz under an AC voltage of 1.0 V_{rms}. The temperature coefficient of capacitance (TCC) was evaluated in the temperature range of -55°C to 125°C using the same LCR meter at a fixed frequency of 1 MHz and 1.0 V_{rms} within a temperature chamber.

Insulation resistance was measured using a high resistance meter (HP 4339B) under an applied voltage of 100 V for 60 seconds at both 25°C and 125°C. The crystal structure of the ceramics was analyzed using X-ray diffraction (XRD, BRUKER, D8, ADVANCE) over a 2θ range of 20° to 70°. Microstructural analysis was performed using scanning electron microscopy (FE-SEM, JSM-9701, JEOL).

3. RESULTS AND DISCUSSION

The calcination temperature and duration for $(Ba_{0.24}Ca_{0.16}Sr_{0.6})(Ti_xZr_{1-x})O_3$ powder are critical parameters that significantly influence particle size distribution and crystallinity, which are pivotal for the reliable fabrication of MLCCs. Based on thermogravimetric (TG) and differential thermal analysis (DTA) results reported in prior studies [13], and considering the stringent requirements for particle size uniformity and crystallinity in MLCC production, the calcination conditions were optimized to 1,150°C for 2 hours. Subsequently, the powder was subjected to a controlled milling process, resulting in a final particle size (D_{50}) of 0.2 ~ 0.3 μm and a specific surface area of 5.5 ~ 6.5 m^2/g, thereby confirming its suitability for high-performance MLCC applications.

Figure 1 shows the XRD analysis results of $(Ba_{0.24}Ca_{0.16}Sr_{0.6})(Ti_xZr_{1-x})O_3$ ceramics sintered at 1,320°C for 4 hours as a function of the Ti/Zr ratio. The XRD patterns indicate that the primary phase is orthorhombic (Pnma), as confirmed by comparison with the standard JCPDS patterns for $BaZrO_3$ (JCPDS: 074-1299), $SrZrO_3$ (JCPDS: 44-0161), $CaZrO_3$ (JCPDS: 35-0645), and $SrTiO_3$ (JCPDS: 35-0734). With increasing Ti^{4+} content, the formation of $(BaCaSr)ZrO_3$ is observed, while a portion of the composition transitions to $(BaCaSr)TiO_3$. When the Ti content reaches 0.35 mol, a secondary phase corresponding to Sr_2TiO_4 and TiO_2 appears, as Sr partially deviates from the $(BaCaSr)ZrO_3$ matrix, disrupting the stoichiometric balance of SrZrO. The analysis of the XRD results as a function of the Ti/Zr ratio reveals that

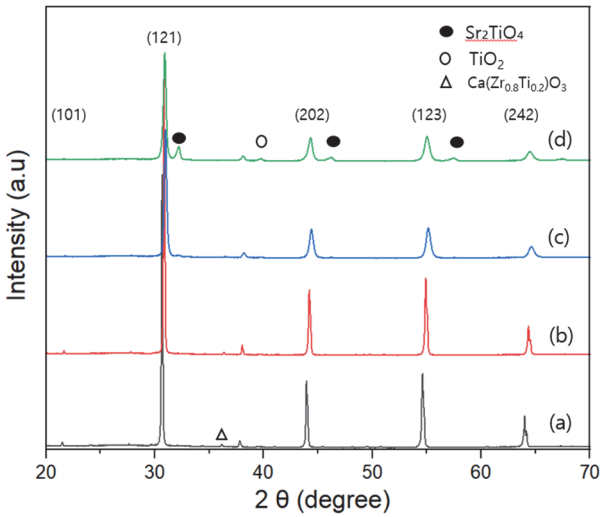

Fig. 1. XRD diffraction pattern according to the Ti/Zr mol ratio in $(Ba_{0.24}Ca_{0.16}Sr_{0.6})(Ti_xZr_{1-x})$ ceramic. (a) x=0.05, (b) x=0.15, (c) x=0.25, and (d) x=0.35.

Ti^{4+} (ionic radius: 0.605 Å), which has a smaller ionic radius compared to Zr^{4+} (ionic radius: 0.72 Å), causes the main peak (121) to shift to higher 2θ angles with increasing Ti^{4+} content, indicating a reduction in unit cell volume.

Figure 2 shows the SEM analysis results of $(Ba_{0.24}Ca_{0.16}Sr_{0.6})(Ti_xZr_{1-x})O_3$ ceramics sintered at 1,320°C for 4 hours as a function of the Ti/Zr ratio. The microstructure observed across all Ti/Zr ratios exhibits uniform grain sizes and low porosity. A trend of decreasing grain size with increasing Ti content was identified. In the range of X = 0.05 to 0.15, the grain size remains uniform, ranging from 1.5 to 2 μm, indicating consistent grain growth. From X = 0.25 onwards, the grain size decreases to 0.3 to 0.6 μm, while maintaining uniformity. These results suggest that Ti ions play a role in inhibiting grain growth. Particularly at X = 0.35, as corroborated by the XRD results shown in Fig. 1, the substitution of Ti^{4+} ions into the B-site of the ABO_3 structure leads to the formation of secondary phases, which influence grain growth. This demonstrates that the substitution of Ti^{4+} ions not only affects grain growth but also induces structural changes that contribute to the observed microstructural evolution.

Figure 3 shows the dielectric constant and dielectric loss of $(Ba_{0.24}Ca_{0.16}Sr_{0.6})(Ti_xZr_{1-x})O_3$ ceramics sintered at 1,320°C for 4 hours as a function of the Ti/Zr ratio. The dielectric constant exhibits a linear increase with the increasing Ti content. In

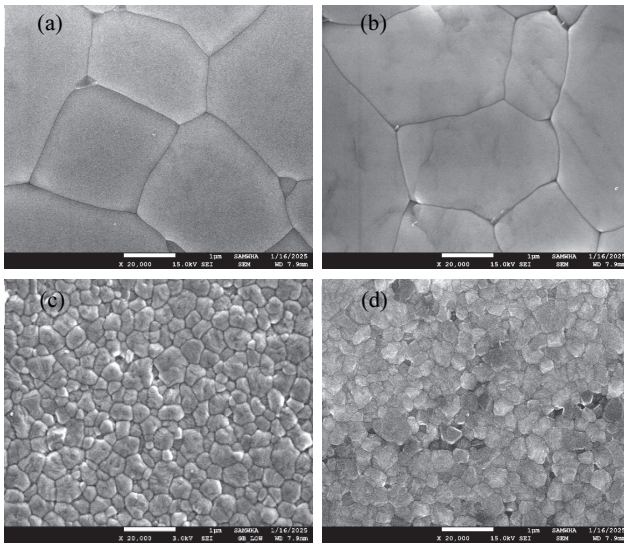

Fig. 2. SEM image patterns according to the Ti/Zr mol ratio in $(Ba_{0.24}Ca_{0.16}Sr_{0.6})(Ti_xZr_{1-x})$ ceramic by sintered at 1,320°C for 2 hr. (a) x=0.05, (b) x=0.15, (c) x=0.25, and (d) x=0.35.

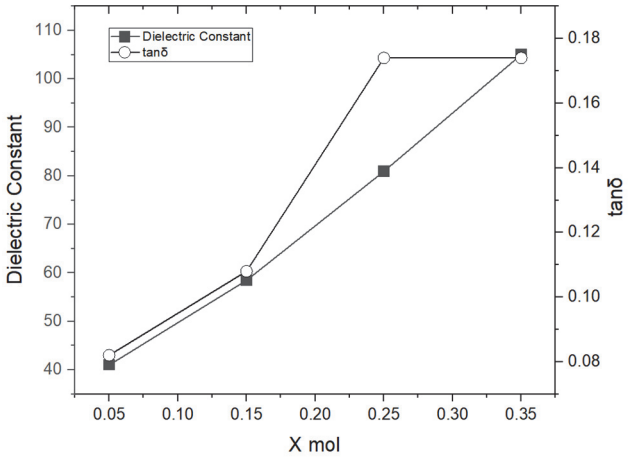

Fig. 3. Dielectric constant and dielectric loss according to the Ti/Zr mol ratio in $(Ba_{0.24}Ca_{0.16}Sr_{0.6})(Ti_xZr_{1-x})$ ceramic.

general, the dielectric constant is significantly influenced by microstructural factors such as the density and porosity of the sintered body. However, as observed in the microstructure shown in Fig. 2, the effects of sinterability and porosity on the dielectric constant are deemed negligible. The increase in the dielectric constant with Ti content is likely due to the lattice distortion caused by the substitution of Zr by Ti, as indicated by the XRD results in Fig. 1. This distortion arises from differences in the ionic radii and bond strengths between Ti and Zr, leading to an increase in the polarizability of the material and, consequently, the dielectric constant. Additionally, as the Ti content increases, the proportion of Zr-based phases such as $CaZrO_3$, $BaZrO_3$, and $SrZrO_3$ decreases, while the proportion of TiO_2 and $SrTiO_3$ phases, which possess relatively higher dielectric constants, increases. Notably, $SrTiO_3$ is a material with an exceptionally high dielectric constant. This phase transformation significantly influences the increase in the overall dielectric constant, consistent with the mixed logarithmic rule [14]. Dielectric loss tends to increase with the increasing Ti content. Generally, as the dielectric constant increases, lattice distortions caused by lattice defects or secondary phases contribute to higher dielectric losses. With increasing Ti content, the relatively low-loss Zr-based phases such as $CaZrO_3$ and $SrZrO_3$ are progressively replaced by TiO_2 and $SrTiO_3$, which exhibit relatively higher dielectric losses. This transition is believed to be the primary factor contributing to the observed increase in dielectric loss.

Figure 4 illustrates the insulation resistance of $(Ba_{0.24}Ca_{0.16}Sr_{0.6})(Ti_xZr_{1-x})O_3$ ceramics sintered at 1,320°C for 4 hours as a function of the Ti/Zr ratio. It shows a tendency for the insulation resistance to decrease with increasing Ti content, and it can be observed that the insulation resistance at high temperatures (125°C) is lower than at room temperature. The decrease in insulation resistance at high temperatures is significantly influenced by impurity levels caused by lattice defects, particularly oxygen vacancies. The reduction in insulation resistance with increasing Ti content can be explained by Eq. (1), which describes the behavior of insulation resistance in a reducing atmosphere with low oxygen partial pressure. In this process, oxygen vacancies ($Vo^{\cdot\cdot}$) and electrons (e^-) are generated as follows: As the Ti content increases, oxygen vacancies are formed, and titanium ions accept electrons, resulting in a change in their oxidation state. Through the reaction shown in Eq. (1) under a reducing atmosphere and the process described in Equation (2), the increase in oxygen vacancies and the oxidation state change of titanium ions are considered the main causes of the decrease in insulation resistance.

$$O_O \rightarrow 1/2\ O_2\ (g) + Vo^{\cdot\cdot} + 2e^- \quad (1)$$

$$O_O + Ti_{Ti}{}^{\times} \rightarrow Vo^{\cdot\cdot} + 1/2\ O_2\ (g) + Ti_{Ti} \quad (2)$$

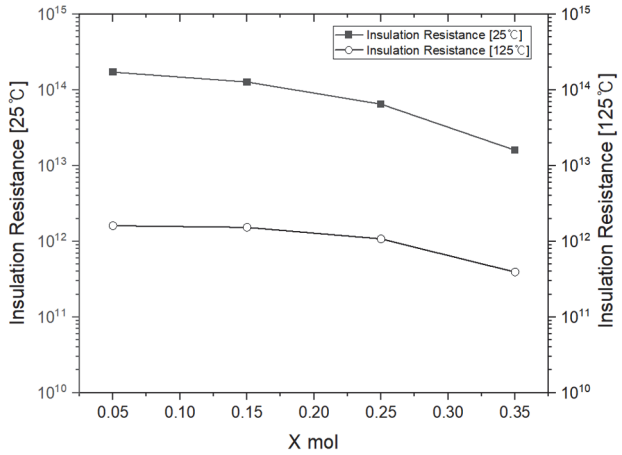

Fig. 4. Insulation Resistance according to the Ti/Zr mol ratio in $(Ba_{0.24}Ca_{0.16}Sr_{0.6})(Ti_xZr_{1-x})$ ceramic.

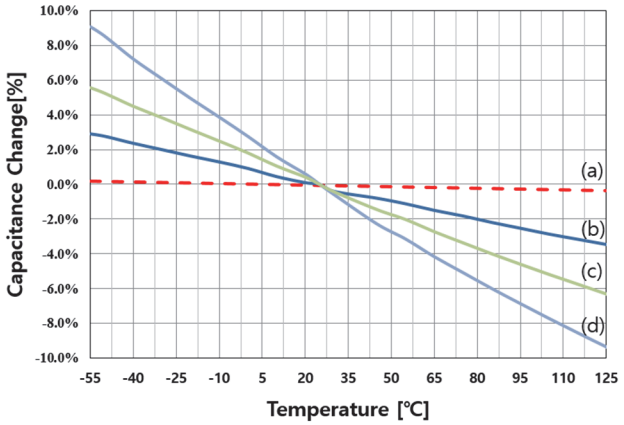

Fig. 5. TCC according to the Ti/Zr mol ratio in $(Ba_{0.24}Ca_{0.16}Sr_{0.6})(Ti_xZr_{1-x})$ ceramic by sintered at 1,320°C for 2 hr. (a) x=0.05, (b) x=0.15, (c) x=0.25, and (d) x=0.35.

Here, Oo represents the oxygen in the $(BaCaSr)(ZrTi)O_3$ composition, $Vo^{\cdot}$: positively charged oxygen vacancy, 1/2 O_2: oxygen released in gaseous form, e^{-}: free electron, $Ti_{Ti}^{\times}$: titanium ion in its normal state as Ti^{4+} and $Ti_{Ti}^{\cdot}$: titanium ion reduced to Ti^{3+} by accepting an electron. To control the oxygen vacancies generated by Eqs. (1) and (2), Mn, Al, and Mo ions contribute to improving insulation resistance characteristics through the mechanisms described in Eqs. (3), (4), and (5). In this study, it was confirmed that as the Ti/Zr ratio increases, optimizing the addition of Al_2O_3 and MoO_3 is necessary to effectively control B-site oxygen vacancies.

$$Mn^{\times}_{Ba/Sr/Ca} + Vo^{\cdot\cdot} + 2e^{-} \rightarrow Mn^{\times\prime\prime}_{Ba/Sr/Ca}$$

$$Mn^{\times}_{Ti} + Vo^{\cdot\cdot} + e^{-} \rightarrow Mn'_{Ti} \quad (3)$$

$$2Al^{\times}_{B\text{-site}} + Vo^{\cdot\cdot} \rightarrow 2Al'_{B\text{-site}} \quad (4)$$

$$Mo^{\times}_{B\text{-site}} + Vo^{\cdot\cdot} + e^{-} \rightarrow Mo'_{B\text{-site}} \quad (5)$$

To compensate for the oxygen vacancies described in Eq. (1), manganese (Mn) was introduced as a dopant. Mn ions occupy both A-site (Ba, Sr, Ca) and B-site (Ti) positions, where their valence state transitions help reduce oxygen vacancy formation. In the A-site, Mn ions capture free electrons and fill oxygen vacancies, while in the B-site, they substitute for Ti and contribute to charge compensation. During the sintering process, the solubility of Mn decreases as the Ti^{4+} content increases, which is believed to contribute to a reduction in insulation resistance. To counteract this effect, molybdenum (Mo^{6+}) ions were used as an additive, as they are reduced to Mo^{4+} or Mo^{3+} and substitute either A-site or B-site ions, thereby stabilizing valence states and enhancing insulation resistance. Additionally, Al^{3+} ions play a crucial role in suppressing conductive electrons at high temperatures when an electric field is applied, which contributes to improving the long-term insulation resistance and lifetime characteristics of MLCCs. These findings highlight the necessity of optimizing Al_2O_3 and MoO_3 additions to effectively control B-site oxygen vacancies and maintain high insulation resistance in MLCCs [15,16].

Figure 5 illustrates the Temperature Coefficient of Capacitance (TCC) of $(Ba_{0.24}Ca_{0.16}Sr_{0.6})(Ti_xZr_{1-x})O_3$ ceramics sintered at 1,320°C for 4 hours as a function of the Ti/Zr ratio. MLCCs are categorized into Class I and Class II based on their temperature characteristics. Class I MLCCs exhibit minimal capacitance variation with temperature changes and are referred to as "temperature compensation capacitors," with C0G (temperature range: -55°C to 125°C, capacitance variation within ±30 ppm/°C) and U2J (temperature range: -55°C to 125°C, capacitance variation between +730 ppm/°C and -750 ppm/°C) being representative specifications. C0G MLCCs typically exhibit small capacitance values, ranging from a few pF to several nF, and are characterized by low loss in high-frequency regions, making them suitable for use in RF circuits. At a Ti content of 0.05, C0G characteristics are

observed, while at a Ti content of 0.15, U2J temperature characteristics become evident. Compared to C0G MLCCs, U2J MLCCs are designed for higher capacitance values, generally ranging from 1 nF to 100 nF. These capacitors are suitable for applications requiring tolerance for slight temperature variations, large capacitance, and operation under high-temperature conditions. Typical applications include automotive inverter circuits and wireless charging systems. The observed increase in TCC with higher Ti content corresponds to the general relationship between dielectric constant (ε_r) and polarizability (α), as expressed in Eq. (6):

$$TC_\varepsilon = \frac{\varepsilon_r}{3}\left(\frac{1}{\alpha}\frac{\partial \alpha}{\partial T} - 3\alpha_L\right) \quad (6)$$

Here, α_L represents the thermal expansion coefficient of the ceramic. The increase in TCC with higher Ti content can be attributed to the rise in the dielectric constant, which intensifies the temperature sensitivity of polarizability, consistent with this theoretical relationship.

4. CONCLUSION

In this study, we developed a dielectric composition suitable for high-capacitance multilayer ceramic capacitors (MLCCs) with temperature compensation characteristics (C0G and U2J characteristics) under reducing conditions. The composition was based on $(Ba_{0.24}Ca_{0.16}Sr_{0.6})(Ti_xZr_{1-x})O_3$, with the Ti/Zr molar ratio adjusted to achieve a dielectric constant ranging from 41.2 to 105, a dielectric loss between 0.0082 and 0.0174%, and an insulation resistance greater than 1.6×10^{13} ohms (at 25°C). X-ray diffraction (XRD) analysis showed no secondary phases up to 0.25 mol of Ti. However, when the Ti content reached 0.35 mol, secondary phases corresponding to Sr_2TiO_4 and TiO_2 appeared. This was attributed to the partial deviation of Sr from the $(BaCaSr)ZrO_3$ matrix, disrupting the stoichiometric balance of $SrZrO_3$. As the Ti/Zr ratio increased, the temperature coefficient of capacitance (TCC) characteristics transitioned from C0G to U2J, and insulation resistance tended to decrease. Despite this, the increasing dielectric constant facilitated the development of MLCCs with high capacitance and high voltage ratings, demonstrating desirable dielectric and electrical properties.

ORCID
Jung Rag Yoon https://orcid.org/0000-0002-9206-8701

ACKNOWLEDGEMENTS

This work was supported by the Technology Innovation Program (RS-2024-00430833, Development of MLCC commercialization technology for automotive electronics alternative to rare earth for high reliability response) funded by the Ministry of Trade, Industry & Energy (MOTIE, Korea).

REFERENCES

[1] K. Hong, T. H. Lee, J. M. Suh, S. H. Yoon, and H. W. Jang, *J. Mater. Chem. C*, **7**, 9782 (2019). doi: https://doi.org/10.1039/C9TC02921D

[2] I. T. Seo, H. W. Kang, and S. H. Han, *J. Korean Inst. Electr. Electron. Mater. Eng.*, **35**, 103 (2022). doi: https://doi.org/10.4313/JKEM.2022.35.2.1

[3] C. H. Lee and J. R. Yoon, *J. Ceram. Process. Res.*, **23**, 181 (2022). doi: https://doi.org/10.36410/jcpr.2022.23.2.181

[4] H. Zheng, I. M. Reaney, D. Mum, T. Price, and D. M. Idoles, *Jpn. J. Appl. Phys., Part 1*, **44**, 3087 (2005). doi: https://doi.org/10.1143/JJAP.44.3087

[5] Y. D. Li, J. M. Chen, and Y. C. Lee, *Ceram. Process. Res.*, **19**, 461 (2018).

[6] T. Yamagushi, Y. Komatsu, T. Otobe, and Y. Murakami, *Ferroelectrics*, **27**, 273 (1980). doi: https://doi.org/10.1080/00150198008226116

[7] Q. Y. Pang, L. Y. Y. Yang, F. Z. W. Liu, X. Li, H. R. Cheng, S. Y. Sun, Y. Chen, and G. S. Wang, *Ceram. Int.*, **49**, 8598 (2023). doi: https://doi.org/10.1016/j.ceramint.2022.11.037

[8] M. Chen, J. L. Liao, and H. I. Hsian, *Ceram. Int.*, **48**, 28023 (2022). doi: https://doi.org/10.1016/j.ceramint.2022.06.107

[9] S. H. Lee, M. K. Kim, H. K. Kim, and J. R. Yoon, *J. Ceram. Process. Res.*, **18**, 722 (2017).

[10] Q. Y. Pang, F. Yang, W. Huang, X. Li, H. R. Cheng, S. Y. Sun, Y. Chen, and G. S. Wang, *J. Mater. Chem. C*, **10**, 16053 (2022). doi: https://doi.org/10.1039/D2TC03756D

[11] J. R. Yoon, S. W. Lee, M. K. Kim, and K. M. Lee, *J. Korean Inst. Electr. Electron. Mater. Eng.*, **21**, 645 (2008). doi: https://doi.org/10.4313/JKEM.2008.21.7.645

[12] C. I. Cheon, J. S. Kim, and H. G. Lee, *J. Mater. Res.*, **13**, 1107 (1998). doi: https://doi.org/10.1557/JMR.1998.0153

[13] H. S. Lee and J. R. Yoon, *J. Korean Inst. Electr. Electron. Mater. Eng.*, **37**, 662 (2024).
doi: https://doi.org/10.4313/JKEM.2024.37.6.13

[14] J. R. Yoon, J. W. Han, K. M. Lee, and H. Y. Lee, *Trans. Electr. Electron. Mater.*, **10**, 116 (2009).

[15] K. Hong, T. H. Lee, J. M. Suh, and J. W. Han, *Electron. Mater. Lett.*, **14**, 629 (2018).
doi: https://doi.org/10.1007/s13391-018-0066-6

[16] C. H. Lee and J. R. Yoon, *J. Ceram. Process. Res.*, **23**, 794 (2022).
doi: https://doi.org/10.36410/jcpr.2022.23.6.794